SIMULATION OF JET AGITATION IN SPRAYER TANKS: COMPARISON OF PREDICTED AND MEASURED WATER VELOCITIES

T. Ucar, R. D. Fox, H. E. Ozkan, R. D. Brazee

ABSTRACT. *FLUENT, a computational fluid dynamics program, was used to investigate flow movements in sprayer tanks with hydraulic jet agitators. Two– and three–dimensional simulations were carried out utilizing single–phase (liquid phase only) and multiphase (solids particles in liquid) models. Earlier experimental studies of agitation effectiveness identified important factors affecting agitation effectiveness. This study was initiated to evaluate simulation as a tool in sprayer agitation system design. Interpretations of the flow field predictions supported previous measurements that determined system pressure to be the most influential factor on agitation effectiveness due to the direct relationship between pressure and jet velocity. Multiphase predictions of particle deposit amounts at the tank bottom were not feasible due to the computational demand of the model, which was an attempt to simulate three–dimensional turbulent flows with solid–liquid mixtures. Quantitative verification of single–phase simulations was accomplished by velocity measurements using hot–film sensors in a sprayer tank. Velocities were measured at 9 locations within the sprayer tank, and 12 jet agitation simulations were used. There were 118 of the 144 measured velocities within 50% of velocities predicted by FLUENT, and 120 of 144 measured velocities were within 0.2 m/s of predicted values. FLUENT–generated values tended to be greater than measured velocities near the top of the tank, and FLUENT velocities were always less than measured velocities at a position near the center of the tank.*

Keywords. *CFD, Simulation, Mixing, Sprayers, Water velocity, Hot–film anemometers.*

Hydraulic agitation in agrochemical sprayer tanks is accomplished by creating a turbulent flow field with a high–velocity jet from agitating nozzles. A pump withdraws part of the fluid from a tank and recycles it through the nozzles. A number of nozzles (up to 8 or more) may be needed in relatively large tanks. The velocity difference between the jet and bulk liquid creates a turbulent mixing layer at the edges of the jet. This layer grows in the direction of the jet, helping entrainment and mixing of jet liquid with bulk liquid. Detailed theory on turbulent jets can be found in Abramovich (1963).

Computational fluid dynamics (CFD) has emerged as a practical tool for many fluid dynamics problems as well as fluid–mixing technology. However, it has been shown that computer storage capacity can significantly affect the accuracy of predictions as well as speed of the machine (Shaw, 1992).

CFD is a numerical solution technique for continuity and momentum equations and conservation equations for energy, chemical species, heat transfer, and chemical reactions in fluid dynamics problems. Navier–Stokes equations for incompressible Newtonian fluids are solved by means of CFD momentum equations. Although numerical models have been successfully applied to solve many fluid dynamics problems, chemical process industries still question CFD because the complex physics of multiphase and viscoelastic flows and reactive chemistry makes these cases difficult to model (Shanley, 1996).

Fluidized bed problems have been the major application area for multiphase flows modeling of solid–liquid mixtures. Harlow and Amsden (1975) described a numerical calculation technique for the solution of multiphase flows where several fields interpenetrated and interacted with each other. In their model, the two fields (solids and fluids) were coupled together through interchanges of mass, momentum, and energy, which were described by several exchange functions. Ding and Gidaspow (1990) derived a predictive two–phase flow model that was a generalization of the Navier–Stokes equations. Gidaspow et al. (1992) used kinetic theory methods to predict flow behavior and oscillations in a complete loop of a circulating fluidized bed. Syamlal et al. (1993) described a multiphase flow model with interphase exchanges to solve chemical reactions and heat transfer in dense or dilute fluid–solid flows. Wang et al. (1997) developed two–fluid turbulence models to describe turbulent gas–solid two–phase flows and derived governing equations as well as kinetic energy dissipation.

In this study, FLUENT (Fluent, Inc., Lebanon, N.H.), a commercial CFD program, was used to predict flow fields and particle suspension/sedimentation in a sprayer tank with jet agitators. Comparisons were made for effect of agitation system design and operating parameters such as jet diameter, orientation, velocity, etc. This study was an extension of previous, experimental research on hydraulic agitation systems in agricultural sprayer tanks conducted in 1996 and

Article was submitted for review in June 2000; approved for publication by the Power & Machinery Division of ASAE in December 2000.

Names are necessary to report factually on available data; however, Ohio State University (OSU) and the USDA neither guarantee nor warrant the standard of the product, and the use of the name by OSU or USDA implies no approval of the product to the exclusion of others that may also be suitable.

The authors are **Tamer Ucar,** ***ASAE Member Engineer***, Assistant Professor, Faculty of Agriculture, University of Yuzuncu Yil, Van, Turkey; **Robert D. Fox**, ***ASAE Member Engineer***, Agricultural Engineer, and **Ross D. Brazee**, ***ASAE Member Engineer***, Senior Research Scientist, USDA Agricultural Research Service, Application Technology Research Unit, OARDC, Wooster, Ohio; and **H. Erdal Ozkan**, ***ASAE Member Engineer***, Professor, FABE, Ohio State University, Columbus, Ohio. **Corresponding author**: Robert D. Fox, USDA–ARS, Agric. Engineering Bldg., 1680 Madison Ave., Wooster, Ohio 44691; phone: 330–263–3871; fax: 330–263–3670; e–mail: fox.8@osu.edu.

1997 (Ucar et al., 2000). In these studies, kaolin clay was used to simulate a dry pesticide in the mixing tests.

Currently, FLUENT utilizes two approaches for the numerical calculation of multiphase flows: the Euler–Lagrange approach and the Euler–Euler approach. Since the Lagrangian model in FLUENT cannot be applied to suspension and sedimentation of solid particles, the Euler–Euler approach with granular (fluid–solid) flow option must be used. In this approach, different phases (solid and fluid) are treated as interpenetrating continua where the sum of phasic volume fractions is equal to one. Conservation equations for each phase are solved by application of kinetic theory (Fluent, 1995).

FLUENT uses the method described by Syamlal and Rogers (1993), by default, for simulating multiphase granular modeling, with an option to choose the model introduced by Ding and Gidaspow (1990) and Gidaspow et al. (1992).

Although commercial CFD software has achieved considerable progress in recent years, multiphase flows are still difficult to model (Myers et al., 1995; Tilton, 1997). Most of the developments in this area have taken place in the nuclear industry, with comparatively little activity in other industrial sectors. That is probably due to the need for further improvement in the models, for example, calculation of the inter–phase drag at high particle loading (Lo et al., 1994). Reasonable solutions, however, may be possible in certain cases, such as well–separated flows and flows in which a second phase appears as discrete particles of known size and shape so that particle motion may be approximated by drag coefficient formulations (Tilton, 1997). Computational methods and commercial CFD packages, including FLUENT, have been used successfully to simulate two– and three–dimensional mixing tanks to study the effects of turbulence and cylindrical tank design on the flow field in mixing vessels (Perng and Murthy, 1992; Togatorop et al., 1994; Armenante and Chou, 1994; Decker and Sommerfeld, 1996).

The first objective of this study was to use the CFD program FLUENT to simulate mixing in agricultural sprayer tanks that employ hydraulic agitation systems. Both single–phase (water velocity fields) and multiphase (movement of solid particles in the established velocity field) computational procedures will be used. The second objective was to compare single–phase computed water velocities within a sprayer tank with water velocities measured with a hot–film anemometer system over the wide range of flow conditions simulated with FLUENT.

Description of the Model and Solution Procedures

FLUENT can model a wide range of physical phenomena, such as fluid flow, heat transfer, and chemical reaction, using conservation equations of mass, momentum, energy, and chemical species using a control volume based, finite difference method. Therefore, the governing equations need to be discretized on a curvilinear grid to enable computations in complex, irregular geometries. To investigate solids suspension and sedimentation in liquids, a submodel of the Eulerian multiphase model included in this software was used. This submodel is called Eulerian granular modeling, or the Euler–Euler approach.

Theory of Eulerian Granular Model Simulations

FLUENT solves a set of conservation of matter and momentum equations for single–phase solutions. When modeling multiphase flow, however, additional sets of conservation equations are needed. Not only these additional equations, but also the original set of equations needs to be modified by considering volume fractions of the phases. The development of these relationships is given in the Fluent User's Guide (Fluent, 1995). Momentum conservation is expressed separately for both fluid (primary phase) and solid phases to calculate the concentration field in the simulation domain for each phase. In addition, two more quantities are taken into account during iterations. These quantities are represented by momentum exchange coefficients between fluid and solid phases as well as between individual solid particles to consider possible particle–particle collisions.

Preprocessor, GeoMesh, for Geometry and Grid Generation

As indicated before, numerical simulation of fluid requires creation of discrete elements of volumes to be used in computations. Therefore, GeoMesh (ICEM Systems, GmbH, and Fluent, Inc.), a CAD program, was used as a geometry setup and grid generation preprocessor for simulations to run with FLUENT. Body–fitted grids require a domain topology in GeoMesh. This topology consists of interconnected mesh areas or volumes that are called faces in 2D or blocks in 3D, respectively. A domain is either a face containing a quadrilateral/triangular grid or a block containing a hexahedral grid. A topology is how the faces or blocks are connected together to produce a structured or unstructured grid.

Once a domain topology is completed in GeoMesh, the user then specifies the node distribution, sets boundary types, and interpolates the grid to be transferred to FLUENT's CFD solver in a grid file. All these tasks are accomplished with the help of a group of FLUENT–supplied system components that include: a session manager, data translators, a geometry modeler (DDN), a block modeler/grid generator (P–Cube), a grid visualizer (Leo), and a solver interface module.

Simulations for Simplifying the Geometry of Simulated Domain

To reduce the number of nodes to manageable levels, the effect of the eductor part of the jet agitator on the general flow field around the jet was investigated. The eductor is a plastic guide that extends about 10 cm from the jet outlet. It is shaped to create a Venturi effect, so that the water jet from the nozzle entrains a maximum amount of surrounding water and increases total water flow produced by the jet. A total of 12 simulations were conducted with and without eductors for comparison (three jet velocities and two orifice sizes in two groups of tests, with or without an eductor extension). Jets were simulated in 2D domain with a structured, body–fitted

grid. In addition, velocity decay along the jet centerline was predicted to examine the influence of the eductor. These predicted values were then compared with the values obtained from previous researchers' findings and theoretical formulations.

Based on results from preliminary simulations, new grid files were generated with improved grid quality and less–complicated domain topology. A vertical portion of the tank that included only one jet nozzle was selected as the simulation domain. This new geometry modeled 1/8th of the whole tank for an 8–jet configuration or 1/4th of the tank for a 4–jet configuration, which resulted in a computation regime of 33,440 nodes (fig. 1).

The two computers used to carry out the simulations were similar: about 166 MHz Pentium processor, 128 MB RAM, and Windows operating system. During multiphase computations, it was necessary to use a time step of only 0.0001 s to avoid divergence. Efforts to increase the time step by adjustments in the under–relaxation parameters, the number of sweeps using the Line–Gauss–Seidel solver for each equation, and different sweep and marching directions were not successful. Since there was no single dominant flow direction, an alternating sweep direction was found to be workable. Although the multigrid solution technique accelerated the single–phase solution, it did not improve the solution when the Eulerian granular model was enabled.

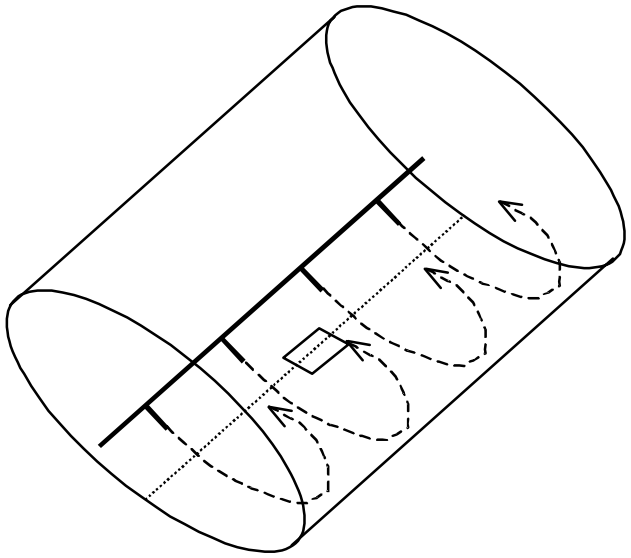

(a)

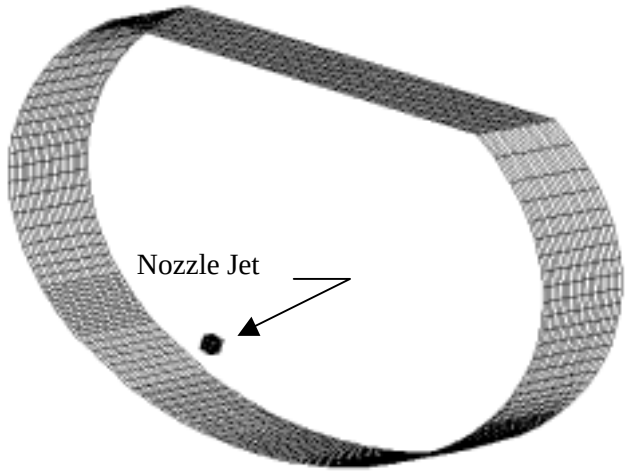

(b)

Figure 1. (a) Illustration of simulated tank showing a system with 4 sequential nozzles, and (b) generated grid for one slice of the tank including only one jet in the computational domain.

Materials and Methods for Validation Experiments

Water velocity measurements were made with a constant–temperature hot–film (CTHF) anemometer in an elliptical, 1136 L sprayer tank. Details on the tank and agitation system are given in Ucar et al. (2000). The anemometer control unit was a TSI model 1010 (St. Paul, Minn.), and sensors used were model 1210–20W (0.005 cm diameter).

For calibration, the sensors were mounted in the center of a plastic pipe with an I.D. of 2.06 cm. Flow through the pipe, measured with an electromagnetic flow meter (Model 38410–EM–05–1/2, Spraying Systems Co., Wheaton, Ill.), was used to calculate actual water velocity in the pipe, based on a turbulent flow regime. A standard non–linear, hot–film regression was calculated and used to convert hot–film output voltages to water velocity. The HF sensor was cleaned after each measurement (2 to 3 min) to reduce error due to contamination of the sensor film by impurities in the water. During calibration, it was found that the cleaning procedure returned the sensor to the original measuring condition.

Velocities were measured at nine points, 3 positions at each of 3 levels, in the sprayer tank, as shown in figure 2. The x– and y–coordinate axes in the tank are also shown in figure 2. The CTHF sensor was mounted on a bracket attached to the tank fill hole, so each position could be reached by rotating the bracket and extending a support arm. All measurements were made in the plane of one of the agitation nozzles. The long axis of the hot–film sensor was aligned with the long axis of the sprayer tank. Thus, the sensor responded mainly to flow in the same plane as the main velocities produced by the agitation nozzle jet. Anemometer voltages were recorded each second for about 2 min. Voltages were converted to velocities using a calibration equation, and then 100 values were averaged to obtain the velocity at each location.

Velocities were measured for the agitating nozzle arrangements shown in table 1. Nozzle arrangements include 3 positions (angled down 30°, down 15°, and level) and 2 system pressures for each position. Each of these 6 treatments was made for 4– and 8–sequential agitation nozzles.

The procedure for measuring water velocity was to start the agitation system, allow it to run for about 30 min to develop steady–state circulation within the tank, and then measure velocities at 9 locations. The agitation system was not stopped during this series of measurements. After each series of measurements, the hot–film sensor was removed, calibration checked, and the sensor cleaned before being placed in the tank for the next set of measurements. All velocity measurements were repeated 3 times. Water veloc–

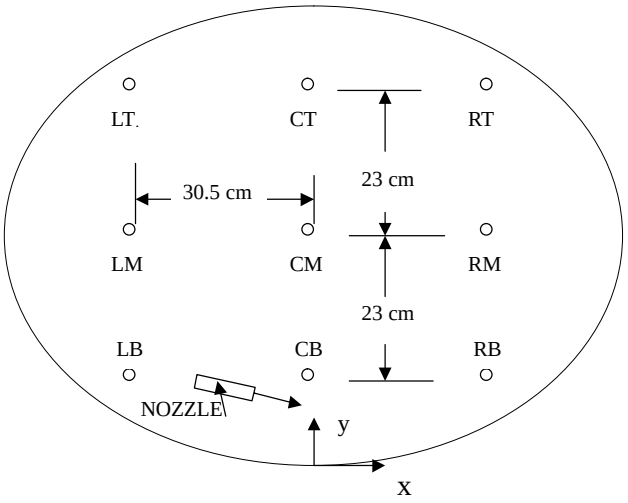

Figure 2. Illustration of the sprayer tank showing velocity measurement positions, viewed from front of sprayer.

Table 1. Agitation system configurations used in water velocity measurement studies; all systems used sequential nozzle configuration.

Test No.	Number of Nozzles	System Pressure (kPa)	Nozzle Angle (° down)	Diameter of Nozzle (mm)
1	8	138	0	3.2
2	8	517	0	3.2
3	8	138	15	3.2
4	8	517	15	3.2
5	8	207	30	4.8
6	8	407	30	4.8
7	4	207	0	3.2
8	4	470	0	3.2
9	4	207	15	3.2
10	4	414	15	3.2
11	4	207	30	4.8
12	4	470	30	4.8

ity values predicted by FLUENT were compared with the 95% confidence interval of measured velocities, based on Student's t distribution.

Selection of Measurement Points in FLUENT Grid

The location of the actual measurement points in the FLUENT grid system was found by using the x, y, and z coordinates given by FLUENT. However, positions on the top row were adjusted slightly by measuring the distance from the top surface of the water in the actual tank to the hot–film sensor. FLUENT velocities at positions the same distance from the top surface of the water boundary were used.

Several factors contributed to difficulty in locating an exact correspondence between tank measurement points and points within the FLUENT–simulated flow field. For ease of changing treatments, actual nozzles were partially supported by plastic tubing. This allowed the nozzles to move slightly when pressure was applied to the system. Slight movement in the jet angle should not affect water velocities in the entire tank, but it could have a significant effect on velocities measured near the jet axis, i.e., those at the bottom positions. In addition, the FLUENT model of the nozzle had very little x–dimension, but the actual nozzle was about 0.11 m long. For positions near the jet orifice, this could introduce errors.

Results and Discussions

2D Simulations for Effect of Eductor on General Flow Field

Using FLUENT simulation, configurations with the same jet velocities and orifice sizes produced similar flow fields both with and without eductors. This indicated that the eductor part of the jet did not affect the general flow field far from the jet. Therefore, the CAD representation of the agitation nozzle was simplified by omitting the eductor.

Fluid Phase Simulations of Jet Agitators in Sprayer Tanks

Experiments by Ucar et al. (2000) showed that four factors were most influential in agitation system effectiveness. Observations of single–phase flow fields for the 35 agitation systems tested were computed using FLUENT. The following paragraphs are based on observations and analysis of these simulated flow fields.

Effect of Jet Angle

As the jet angle increased from 0º (horizontal) to 30º down from horizontal, fluid velocity in the area below the jets decreased by approximately 15–20% for a given jet initial velocity, indicating more susceptibility for kaolin clay to deposit in this area. When the jets were oriented horizontally, jet flow conformed well to the general flow field in the tank, transferring most of the jet energy into the fluid mass. As the jet angle increased, more jet energy was dissipated because the jet was striking the tank bottom within a relatively short distance. In addition, the jet flow crossed streamlines of the fluid mass at an angle. Observations during actual experiments with these jet angles confirmed that sedimentation on the tank bottom usually occurred at locations below and behind the jet agitators (fig. 3).

Effect of System Pressure (Jet Velocity)

Changing the initial jet velocity greatly affected the "magnitude" of velocities in the other locations of the tank, although it did not change the general flow pattern, i.e. flow directions and relative differences in fluid–flow throughout the tank. For example, fluid velocity below the jets near the tank bottom, which was the most critical location in the tank, increased by about 65% as the system pressure increased from 207 to 483 kPa.

Effect of Jet Spacing

Flow fields for wide (4 jets) and narrow (8 jets) spacing options at a cross–section were very similar. However, for the same jet velocity, orifice size, and jet configuration, smaller spacing provided a more uniform velocity field than larger spacing. Narrow jet spacing produced less velocity variation along one slice of the tank, and hence provided better agitation, because more fluid was being injected into the tank with more jet nozzles.

Figure 3. A picture showing clay deposits remaining in the tank bottom after a typical agitation test in a tank with 2840 L capacity. Clay deposition usually occurs off–center at the bottom.

Effect of Jet Orifice Diameter

Using a smaller or larger orifice did not make a difference in the general flow pattern, as was the case for pressure effect. However, a larger orifice greatly increased velocity magnitude in all locations within the tank slice since more fluid was delivered into the domain for the same initial jet velocity with a larger opening.

Multiphase Model Simulations

After a careful investigation of CFD models in FLUENT as a possible tool to study tank mixing phenomenon, it became apparent that simulating sedimentation of solid particles in a liquid phase was not feasible with this technique. This was consistent with other researchers' findings.

Although FLUENT has been successfully used to implement a wide variety of flow models, multiphase flow models have several characteristics that require complicated methods and large computational times (Fluent, 1995). Even though we minimized the number of nodes in the simulation domain, the final model was still too complicated for Eulerian multiphase solutions with turbulent characteristics of the flow. For comparison, a fully converged turbulent single–phase solution for the eight–jet configuration was obtained in 9 hours. However, when FLUENT's Eulerian granular model was activated using already–calculated single–phase flow field data, the model required about one month, running 24 hours a day, to obtain one second of information on water and clay particle movement in the simulated sprayer tank section.

The single–phase computations of the velocity and turbulence distribution in the tank provided valuable information about flow circulation patterns in a sprayer tank that should definitely help manufacturers design more efficient agitation systems.

Additional Considerations

The simulated agitation system shown in figure 1 created a circulation on the vertical plane inside the tank (fig. 4). As discussed above, if circulation speed was not adequate, some solid particles deposited on the tank bottom, just below the jets. That was probably because there wasn't sufficient vertical force on these particles to overcome gravity forces. A possible problem with this type of agitation might be similar to that of vertical mixing vessels. In vertical tanks, a center vortex can form, and the fluid then simply rotates around the vessel instead of mixing vertically. Baffles are placed on the wall inside the tank to prevent this horizontal rotation and to increase vertical movement of the fluid mass (Brodkey and Hershey, 1988). However, in horizontal tanks, a vortex due to this circulation pattern would seem to be unlikely because both sides of the sprayer tank are closed. In addition, solid particles actually need this rotational movement to overcome gravity and move upward. It is very possible that particles start moving downward when they reach the top. Hence, the more–violent circulation would produce the more–uniform mixture in the tank. Of course, there must be a limit for this advantage depending on particle size, viscosity, and density.

Results Of Validation Experiments

Comparisons among water velocities computed with FLUENT single–phase simulations and velocities measured with a CTHF anemometer are shown in tables 2 to 7. Results

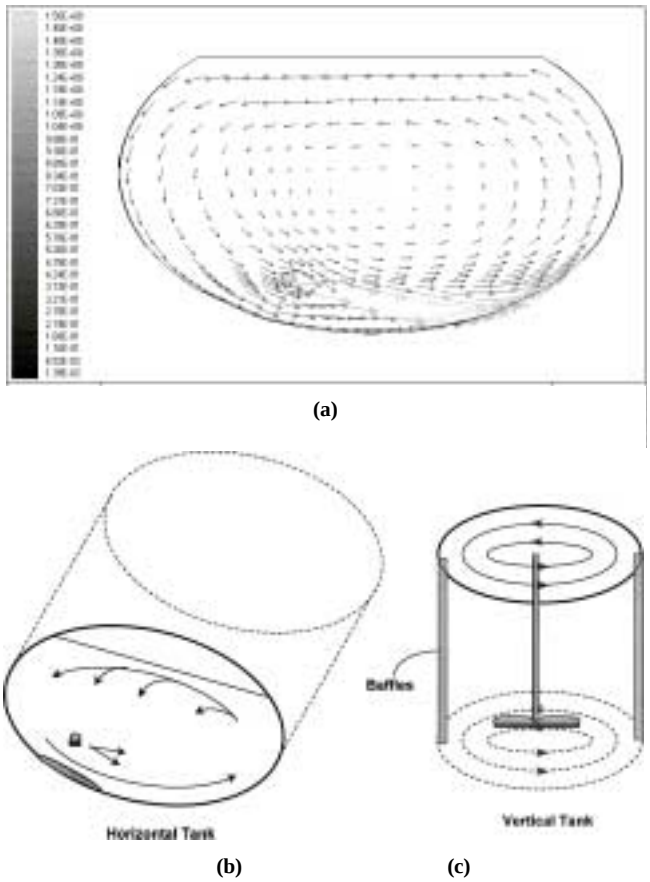

Figure 4. (a) Typical FLUENT output, showing velocity vectors of an agitation system with hydraulic jets, and mixing in (b) horizontal and (c) vertical mixing tanks.

with horizontal nozzles are shown in tables 2 and 3, results with nozzles directed 15° down are shown in tables 4 and 5, and results with nozzles directed 30° down are shown in tables 6 and 7.

Water velocity gradients varied greatly in the sprayer tank during agitation. The greatest gradients were near nozzle outlets and along the main jet from the nozzles. Other locations with fairly large gradients were near the walls of the tank and near the top surface. To match measurement positions as closely as possible with FLUENT positions, the distance from the water surface to the top row of measurement points was measured, and FLUENT velocities were chosen for locations the same distance below the water surface. Velocities were measured and computed when there was about 950 L of water in the tank.

Table 2. Comparison of water velocities predicted using FLUENT with measured velocities. Four sequential nozzles, angle horizontal.

	3.2 mm Orifice, 207 kPa					3.2 mm Orifice, 470 kPa				
	Measured Velocity		FLUENT Velocity	Difference[a] $V_F - V_m$		Measured Velocity		FLUENT Velocity	Difference[a] $V_F - V_m$	
Position	(m/s)	COV	(m/s)	(m/s)	(%)	(m/s)	COV	(m/s)	(m/s)	(%)
LB	0.11	2.32	0.23	0.12	52	0.22	3.47	0.36	0.14	39
CB	0.33	15.45	0.73	0.40	55	0.75	3.36	1.1	0.35	32
RB	0.33	4.28	0.87	0.54	62	0.76	5.05	0.87	0.11	13
LM	0.07	15.65	0.12	0.05	42	0.11	6.72	0.17	0.06	35
CM	0.10	10.21	0.07	–0.03	–43	0.14	21.98	0.10[b]	–0.04	–40
RM	0.10	1.28	0.08	–0.02	–25	0.15	25.14	0.13[b]	–0.02	–15
LT	0.12	2.54	0.24	0.12	50	0.22	12.63	0.34	0.12	35
CT	0.17	2.96	0.29	0.12	41	0.38	10.98	0.44[b]	0.06	14
RT	0.14	2.38	0.21	0.07	33	0.31	17.22	0.31[b]	0.00	00

[a] V_F = FLUENT velocity, V_m = measured velocity.
[b] FLUENT velocities within the 95% confidence interval of measured velocities, based on Student's t–distribution.

Table 3. Comparison of water velocities predicted using FLUENT with measured velocities. Eight sequential nozzles, angle horizontal.

	3.2 mm Orifice, 138 kPa					3.2 mm Orifice, 517 kPa				
	Measured Velocity		FLUENT Velocity	Difference[a] $V_F - V_m$		Measured Velocity		FLUENT Velocity	Difference[a] $V_F - V_m$	
Position	(m/s)	COV	(m/s)	(m/s)	(%)	(m/s)	COV	(m/s)	(m/s)	(%)
LB	0.09	16.52	0.25	0.16	64	0.28	18.98	0.51	0.23	45
CB	0.55	5.31	0.49[b]	–0.06	–12	1.11	9.34	0.98[b]	–0.13	–13
RB	0.21	9.78	0.39	0.18	46	0.41	8.40	0.79	0.38	48
LM	0.07	6.88	0.14	0.07	50	0.18	8.53	0.28	0.10	36
CM	0.09	5.73	0.07	–0.02	–29	0.30	15.99	0.14	–0.16	–114
RM	0.11	10.03	0.12[b]	0.01	8	0.24	23.28	0.24[b]	0	0
LT	0.13	10.25	0.25	0.12	48	0.26	38.29	0.51	0.25	49
CT	0.22	7.93	0.34	0.12	35	0.38	24.49	0.69	0.31	45
RT	0.18	1.17	0.24	0.06	25	0.33	15.59	0.49	0.16	33

[a] V_F = FLUENT velocities, V_m = measured velocities.
[b] FLUENT velocities within the 95% confidence interval of measured velocities, based on Student's t–distribution.

Table 4. Comparison of water velocities predicted using FLUENT with measured velocities. Four sequential nozzles, angle 15° down.

	3.2 mm Orifice, 207 kPa					3.2 mm Orifice, 414 kPa				
	Measured Velocity		FLUENT Velocity	Difference[a] $V_F - V_m$		Measured Velocity		FLUENT Velocity	Difference[a] $V_F - V_m$	
Position	(m/s)	COV	(m/s)	(m/s)	(%)	(m/s)	COV	(m/s)	(m/s)	(%)
LB	0.16	1.21	0.21	0.05	24	0.25	1.37	0.31	0.06	19
CB	1.43	0.78	0.34	–1.09	–321	2.04	1.94	0.49	–1.55	–316
RB	0.48	8.46	0.27	–0.21	–79	0.82	2.26	0.39	–0.43	–110
LM	0.10	5.43	0.08	–0.02	–25	0.13	10.64	0.12[b]	–0.01	–8
CM	0.12	6.13	0.05	–0.07	–140	0.17	6.29	0.07	–0.10	–143
RM	0.07	4.67	0.07[b]	0	0	0.10	13.69	0.11[b]	0.01	9
LT	0.07		0.24	0.17	71	0.11	15.34	0.35	0.24	69
CT	0.15	12.44	0.29	0.14	48	0.23	3.97	0.42	0.19	45
RT	0.12	8.61	0.24	0.12	50	0.13	5.69	0.34	0.21	62

[a] V_F = FLUENT velocities, V_m = measured velocities.
[b] FLUENT velocities within the 95% confidence interval of measured velocities, based on Student's t–distribution.

Velocities at the bottom row of points were subject to large velocity gradients near the main jet of water from the nozzles. We measured a y–z profile of velocities at the x coordinate of position RB opposite the nozzle (see fig. 2) to locate the maximum velocity for treatment 12 (4 nozzles horizontal, 470 kPa, 3.2 mm orifice). The maximum velocity in the FLUENT grid system near position RB was also determined by inspection using the velocity tables. Then y–z coordinates equal to the measured maximum velocity offset were used to select the y and z grid points for obtaining water velocity from the FLUENT tables for all treatments at the bottom level. At the y–z plane near position RB, the measured maximum average velocities for 1 s and 1 min were 1.4 m/s and 0.8 m/s, respectively. Maximum velocity calculated with FLUENT on the same x plane was 0.93 m/s.

Student's t–distribution was used to identify treatments in which the velocities calculated using FLUENT were within the 95% confidence interval of the measured velocity at each point. Only 33 of 144 predicted velocity treatments were within the 95% confidence limits, but 21 other treatments had

Table 5. Comparison of water velocities predicted using FLUENT with measured velocities. Eight sequential nozzles, angle 15° down.

	3.2 mm Orifice, 138 kPa					3.2 mm Orifice, 517 kPa				
	Measured Velocity		FLUENT Velocity	Difference[a] $V_F - V_m$		Measured Velocity		FLUENT Velocity	Difference[a] $V_F - V_m$	
Position	(m/s)	COV	(m/s)	(m/s)	(%)	(m/s)	COV	(m/s)	(m/s)	(%)
LB	0.12	34.30	0.35	0.23	66	0.30	5.98	0.51	0.21	41
CB	0.23	9.97	0.34	0.11	32	0.45	17.90	0.52[b]	0.07	13
RB	0.10	20.07	0.44	0.34	77	0.27	19.08	0.67	0.40	60
LM	0.06	14.60	0.12	0.06	50	0.19	17.27	0.17[b]	–0.02	–12
CM	0.16	6.12	0.07	–0.09	–129	0.40	25.58	0.11	–0.29	–264
RM	0.06	6.02	0.12	0.06	50	0.23	20.37	0.19[b]	–0.04	–21
LT	0.18	11.50	0.35	0.17	49	0.42	11.58	0.58	0.16	28
CT	0.26	9.89	0.43	0.17	40	0.80	11.23	0.68[b]	–0.12	–18
RT	0.22	27.32	0.41	0.19	46	0.63	18.36	0.62[b]	–0.01	–2

[a] V_F = FLUENT velocities, V_m = measured velocities.
[b] FLUENT velocities within the 95% confidence interval of measured velocities, based on Student's t–distribution.

Table 6. Comparison of water velocities predicted using FLUENT with measured velocities. Four sequential nozzles, angle 30° down.

	4.8 mm Orifice, 207 kPa					4.8 mm Orifice, 470 kPa				
	Measured Velocity		FLUENT Velocity	Difference[a] $V_F - V_m$		Measured Velocity		FLUENT Velocity	Difference[a] $V_F - V_m$	
Position	(m/s)	COV	(m/s)	(m/s)	(%)	(m/s)	COV	(m/s)	(m/s)	(%)
LB	0.19	9.87	0.27	0.08	30	0.35	7.96	0.42[b]	0.07	17
CB	0.07	3.31	0.22	0.15	68	0.17	27.73	0.34	0.17	50
RB	0.09	12.35	0.24	0.15	63	0.26	15.13	0.37	0.11	30
LM	0.08	7.64	0.10	0.02	20	0.17	5.66	0.15[b]	–0.02	–13
CM	0.11	4.23	0.06	–0.05	–83	0.15	29.28	0.09[b]	–0.06	–67
RM	0.10	18.64	0.10[b]	0	0	0.14	15.10	0.15[b]	0.01	7
LT	0.16	10.37	0.28	0.12	43	0.14	11.99	0.44	0.30	68
CT	0.27	32.07	0.35[b]	0.08	23	0.28	14.39	0.54	0.26	48
RT	0.25	9.78	0.31	0.06	19	0.29	15.24	0.49	0.20	41

[a] V_F = FLUENT velocities, V_m = measured velocities.
[b] FLUENT velocities within the 95% confidence interval of measured velocities, based on Student's t–distribution.

Table 7. Comparison of water velocities predicted using FLUENT with measured velocities. Eight sequential nozzles, angle 30° down.

	4.8 mm Orifice, 207 kPa					4.8 mm Orifice, 407 kPa				
	Measured Velocity		FLUENT Velocity	Difference[a] $V_F - V_m$		Measured Velocity		FLUENT Velocity	Difference[a] $V_F - V_m$	
Position	(m/s)	COV	(m/s)	(m/s)	(%)	(m/s)	COV	(m/s)	(m/s)	(%)
LB	0.30	46.27	0.29[b]	–0.01	–3	0.45	31.44	0.42[b]	–0.03	–7
CB	0.13	23.62	0.22	0.09	41	0.27	7.26	0.34	0.07	21
RB	0.27	8.45	0.25[b]	–0.02	–8	0.30	13.72	0.39[b]	0.09	23
LM	0.10	27.14	0.09[b]	–0.01	–11	0.18	0.69	0.14	–0.04	–29
CM	0.14	8.91	0.09	–0.05	–56	0.26	3.25	0.09	–0.17	–189
RM	0.14	34.22	0.10[b]	–0.04	–40	0.16	6.23	0.14[b]	–0.02	–14
LT	0.15	12.80	0.15[b]	0	0	0.21	29.75	0.23[b]	0.02	9
CT	0.26	30.67	0.20[b]	–0.06	–30	0.36	20.39	0.30[b]	–0.06	–20
RT	0.17	4.55	0.26	0.09	35	0.25	3.83	0.39	0.14	36

[a] V_F = FLUENT velocities, V_m = measured velocities.
[b] FLUENT velocities within the 95% confidence interval of measured velocities, based on Student's t–distribution.

standard deviations less than 5% of mean velocities. The 95% confidence interval is narrow for small standard deviations.

The difference between measured water velocities and FLUENT predicted velocities at each point is shown is tables 2 to 7, both as an absolute value (m/s) and as a percentage of FLUENT values. Using percent error as a criterion, then 118 of 144 measured values are within ±50% of predicted velocities. Nineteen of the 26 values that differ by more than 50% occur at positions CB and RB, which are near the jet outlet, or at position CM in the center of the tank, where FLUENT velocities were always less than measured values.

Other consistent differences between measured and predicted velocities occurred along the top 3 positions, where FLUENT velocities were nearly always greater than measured velocities. These differences, along with those at the center position (CM), may be due to the corrugations in the tank sidewalls, which induced turbulence into the flow. Increased turbulence may have increased the flow near the center of the tank and decreased flow near the top of the tank.

Large differences in measured and expected flow were observed for the 4–nozzle, 15° down treatments in the bottom center of the tank (see tables 4 and 5). This position was only about 10 cm from the nozzle outlet, so the jet was quite narrow. Thus, an error in sampling position or alignment of the nozzle can lead to large velocity changes. In these cases, maximum velocities calculated by FLUENT were nearly equal to those measured, but they occurred about 3 cm from the measurement location.

These comparisons show that the velocity field predicted by FLUENT is a reasonable approximation to actual water flow in a sprayer tank.

Conclusions

1. Multiphase granular modeling of 3D simulations for tank agitation (33440 nodes), in a usable time frame, would require computational speeds about 5,000 times faster than the 166 MHz machine used in this study.
2. Single–phase simulations of hydraulic jet agitation systems provided useful information about mean velocity fields in mixing tanks. Observations of 35 flow field simulations of different agitation systems supported experimental agitation results reported by Ucar et al. (2000).
3. Most measured water velocities (118 of 144) were within 50% of values computed using FLUENT for flow fields in a sprayer tank with hydraulic agitation. Predicted values were reasonable approximations for velocities measured with hot–film sensors at most positions in the tank.

Acknowledgements

The authors thank A. A. Doklovic for setting up mechanical equipment on the sprayer tank, including the positioner for the hot–film sensor, and B. E. Nudd and K. A. Williams for carefully measuring water velocities with the hot–film sensors.

References

Abramovich, G. N. 1963. *The Theory of Turbulent Jets*. Cambridge, Mass.: Massachusetts Institute of Technology.

Armenanta, P. M., and C. C. Chou. 1994. Experimental LDV measurement and numerical CFD determination of the fluid velocity distribution in an unbaffled mixing vessel. In *Industrial Mixing Technology: Chemical and Biological Application*. AIChE Symp. Series 299, Vol. 90: 33–40.

Brodkey, R. S., and H. C. Hershey. 1988. *Transport Phenomena, A Unified Approach*. New York, N.Y.: McGraw–Hill.

Decker, S., and M. Sommerfeld. 1996. Calculation of particle suspension in agitated vessels with the Euler–Lagrange approach. In *Symp. Series* No. 140: 71–82. Bedford, U.K.: Institution of Chemical Engineers.

Ding, J., and D. Gidaspow. 1990. A bubbling fluidization model using kinetic theory of granular flow. *Am. Inst. Chem. Eng. J.* 36(4): 523–538.

Fluent. 1995. *Fluent User's Guide*. Version 4.3. Lebanon, N. H.: Fluent, Inc.

Gidaspow, D., R. Bezburuah, and J. Ding. 1992. Hydrodynamics of circulating fluidized beds: Kinetic theory approach. In *Fluidization VII: Proceedings of the Seventh Engineering Foundation Conference on Fluidization*, 75–82. Brisbane, Australia. New York, N.Y.: Engineering Foundation Conferences.

Harlow, F. H., and A. A. Amsden. 1975. Numerical calculation of multiphase fluid flow. *J. Computational Physics* 17: 19–52.

Lo, S. M., M. Hannan, N. Hallas, I. P. Jones, and N. S. Wilkes. 1994. Multi–phase CFD applications in the process industry. In *9th Annual Conference of the International Hightech–Forum Basel*. Second World Conference in Applied Computational Fluid Dynamics, Basel, Switzerland. World User Association in Applied Computational Fluid Dynamics.

Myers, K. J., A. Bakker, and J. Fasano. 1995. Simulation and experimental verification of liquid–solid agitation performance. In *Am. Inst. Chem. Eng. Symp. Series 305: Industrial Mixing Fundamentals with Applications*. G. B. Tatterson, R. V. Calabrese, and W. R. Penney, eds. Vol. 91: 139–145.

Perng, C. Y., and J. Y. Murthy. 1992. A Moving–Mesh Technique for Simulation of Flow in Mixing Tanks. Fluent, Inc. TN–38. Presented at the AIChE Ann. Meeting, Nov. 1992, Miami Beach, Fla.

Shanley, A. 1996. Pushing the limits of CFD. *Chem. Eng.* December: 66–67.

Shaw, C. T. 1992. *Using Computational Fluid Dynamics*. Paramus, N.J.: Prentice Hall International, Inc.

Syamlal, M., W. Rogers, and O'Brien, T. J. 1993. *MFIX Documentation Theory Guide*. Technical Note. Morgantown, West Virginia: Morgantown Energy Technology Center, Office of Fossil Energy, U.S.D.E. NTIS/DE94000087. Springfield, Va.: National Technical Information Service.

Tilton, J. N. 1997. Fluid and particle dynamics. In *Perry's Chemical Engineer's Handbook*, 7th ed. R. H. Perry and D.W. Green, eds. New York, N.Y.: McGraw Hill.

Togatorop, A., R. Mann, and D. F. Schofield. 1994. An application of CFD to inert and reactive tracer mixing in a batch stirred vessel. In *Industrial Mixing Technology: Chemical and Biological Application.* AIChE Symp. Series 299, Vol. 90: 19–32.

Ucar, T., H. E. Ozkan, R. D. Fox, R. D. Brazee, and R. C. Derksen. 2000. Experimental study of jet agitation effects on agrochemical mixing in sprayer tanks. *J. Agric. Eng. Res.* 75(2): 195–207.

Wang, Y., S. Komori, and M. K. Chung. 1997. A two–fluid turbulence model for gas–solid two–phase flows. *J. Chem. Eng. Japan* 30(3): 526–534.